Case Studies in Thermal Engineering 3 (2014) 59–67

Contents lists available at ScienceDirect

Case Studies in Thermal Engineering

journal homepage: www.elsevier.com/locate/csite

Heat transfer augmentation in the straight channel by using nanofluids

M.Kh. Abdolbaqi [a,*], C.S.N. Azwadi [b], R. Mamat [a]

[a] Faculty of Mechanical Engineering, 26600 Pekan, Pahang, University Malaysia Pahang, Malaysia
[b] Faculty of Mechanical Engineering, 81200 Skudai, Johor Bahru, Universiti Teknologi Malaysia, Malaysia

ARTICLE INFO

Article history:
Received 29 March 2014
Received in revised form
16 April 2014
Accepted 17 April 2014
Available online 24 April 2014

Keywords:
Nanofluid
Heat transfer
Straight channel
CFD
FLUENT

ABSTRACT

Heat transfer enhancement of nanofluids under turbulent flow through a straight square channel under constant heat flux conditions at the upper and lower walls is studied numerically. The nanofluids are prepared as solid nanoparticles of CuO, TiO_2 and Al_2O_3 suspended in water. CFD analysis by FLUENT software using the finite volume method is conducted. The boundary conditions are applied under a heat flux of 5000 W/m^2, Reynolds numbers of 10^4–10^6 and a constant volume concentration of 1–4%. The results show that the heat transfer rates and wall shear stress increase with an increase of the nanofluids' volume concentration. It seems that the CuO nanofluid significantly enhances heat transfer. The results show good agreement with results of other researchers by a 10% deviation.

1. Introduction

Many applications of heat transfer enhancement using nanofluids to get the cooling challenge necessary such as the photonics, transportation, electronics, and energy supply industries [1–4]. Hussein et al. [5] studied the effect of the SiO_2 nanofluid on an automotive cooling system. Both experiments and simulations by FLUENT software have been adopted. Results showed significant enhancement of the heat transfer with the nanofluids and agreed with the available literature data. Bahiraei et al. [6] examined the effect of temperature and volume fraction on the viscosity of TiO_2–water nanofluid. The results were recorded and analyzed within the temperature range of 25–70 °C and the volume fractions 0.1%, 0.4%, 0.7% and 1%. The viscosity of two different materials, single wall carbon nanohorn (SWCNH) and titanium dioxide (TiO_2), suspended in water was measured experimentally by Bobbo et al. [7]. Empirical correlation equations of viscosity against nanofluid volume fraction have been developed. The forced convection turbulent flow of Al_2O_3–water nanofluid inside an annular tube with variable wall temperatures was investigated experimentally by Prajapati et al. [8]. The results showed that the heat transfer was enhanced due to the nanoparticles dispersed in the fluid. Horizontal double-tube heat exchanger counter turbulent flow was studied numerically by Bozorgan et al. [9]. Al_2O_3–water nanofluid of 7 nm with volume concentration up to 2% was selected as the coolant fluid. The results showed that the pressure drop of the nanofluid is slightly higher than water and increases with the increase of volume concentrations. A double tube coaxial heat exchanger heated by solar energy using aluminum oxide nanofluid was presented experimentally and numerically by Luciu et al. [10]. The results showed that nanofluids have a higher performance of heat transfer than base fluids. The turbulent flow of (CuO, Al_2O_3 and TiO_2) nanofluids with different volume concentrations flowing through a two-dimensional duct under constant heat flux conditions has been analyzed numerically by Rostamani et al. [11].

* Corresponding author.
E-mail address: abdolbaqi.mk@gmail.com (M.Kh. Abdolbaqi).

http://dx.doi.org/10.1016/j.csite.2014.04.001

Nomenclature

C	specific heat [W/kg °C]
D	diameter [m]
E	energy [W]
f	friction factor
htc	convection heat transfer coefficient [W/m^2 °C]
k	thermal conductivity [W/m °C]
Nu	Nusselt number [$htc\ D/K_{nf}$]
P	pressure [N/m^2]
Pr	Prandtl number [$C\mu/K_{nf}$]
Re	Reynolds number [$\rho_{nf}D_h u/K_{nf}$]
u	velocity [m/s]
μ	viscosity [N s/m^2]
ρ	density [kg/m^3]
τ	shear stress [N/m^2]
ϕ	volume concentration

Subscripts

f	liquid phases
p	solid particle
nf	nanofluid
h	hydraulic

In this study, heat transfer enhancement in a straight square channel is carried out. This work contributed to the knowledge of heat transfer enhancement for many industrial applications. CFD analysis by FLUENT software using the finite volume method is adopted. The heat flux, Reynolds numbers and volume concentration are 5000 W/m^2, 10^4–10^6 and 1–4%, respectively. Three types of nanofluids (Al_2O_3, TiO_2 and CuO) dispersed in water are utilized. The results are compared with experimental data available in the literature to be validated.

2. Thermal properties

The density (ρ_{nf}), specific heat capacity (C_{nf}), thermal conductivity (k_{nf}) and viscosity (μ_{nf}) of the nanofluid are obtained by the corresponding relations [12]

$$\rho_{nf} = \left(\frac{\phi}{100}\right)\rho_p + \left(1-\frac{\phi}{100}\right)\rho_f \tag{1}$$

$$C_{nf} = \frac{\frac{\phi}{100}(\rho C)_p + (1-\frac{\phi}{100})(\rho C)_f}{\rho_{nf}} \tag{2}$$

$$k_r = \frac{k_{nf}}{k_f} = 0.8938\left(1+\frac{\phi}{100}\right)^{1.37}\left(1+\frac{T_{nf}}{70}\right)^{0.2777}\left(1+\frac{d_p}{150}\right)^{-0.0336}\left(\frac{\alpha_p}{\alpha_f}\right)^{0.01737} \tag{3}$$

$$\mu_r = \frac{\mu_{nf}}{\mu_f} = \left(1+\frac{\phi}{100}\right)^{11.3}\left(1+\frac{T_{nf}}{70}\right)^{-0.038}\left(1+\frac{d_p}{170}\right)^{-0.061} \tag{4}$$

The assumption of the problem undertaken is that the nanofluid behaves as a Newtonian fluid for a concentration of less than 4.0%. For conditions of dynamic similarity for flow of the two media, nanoparticles and base liquid water, in the channel, the ratio of friction coefficients can be written as follows:

$$f_r = \frac{f_{nf}}{f_f} = \left[\frac{C2}{C3}\right]\frac{Re_f^m}{Re_{nf}^p} \tag{5}$$

For base fluid water [13]

$$f_f = \frac{0.316}{Re^{0.25}} \tag{6}$$

The system of governing criteria can be written as

$$f_r = \frac{f_{nf}}{f_f} = F\left[\frac{\rho_{nf}}{\rho_f}, \frac{\mu_{nf}}{\mu_f}\right] \tag{7}$$

The empirical correlation obtained from experimental data of a number of investigators [14–18] is

$$f_r = \frac{f_{nf}}{f_f} = 1.078\left[\left(\frac{\rho_{nf}}{\rho_f}\right)^{-0.514}\left(\frac{\mu_{nf}}{\mu_f}\right)^{-0.1248}\right] \tag{8}$$

Forced convection heat transfer coefficient under turbulent flow may be estimated by the Dittus–Boelter correlation (Eq. (9)) for pure water in the range of Reynolds number $1\times10^4 < Re < 1\times10^5$.

$$Nu = \frac{h_f}{k_f}D = 0.023\ Re^{0.8}\ Pr^{0.4} \tag{9}$$

The modified Dittus–Boelter equation (10) is applicable for both water and nanofluids with spherical shaped nanoparticles dispersed in water as [14]

$$Nu_{nf} = \frac{h_{nf}}{k_{nf}} D = 0.023\, Re^{0.8}\, Pr_f^{0.4} (1 + Pr_{nf})^{-0.012} (1 + \phi)^{0.23} \tag{10}$$

The Reynolds number depending on the hydraulic diameter of the channel can be defined as

$$Re = \frac{\rho_{nf} D_h u}{\mu_{nf}} \tag{11}$$

Computational fluid dynamics (CFD) has the ability to deal with a wide range of simulating engineering problems related to heat transfer by means of the numerical solution. The CFD problem could be tackled by general procedures: physical scenario, geometry, computational mesh, governing equation, solution algorithm, boundary condition, solution and analysis [6]. After understanding the heat transfer and fluid flow phenomena in the channel, the CFD modeling region could be classified into a few major steps: the preprocess stage, the geometry of the CFD region constructed, and a computational mesh generated in GAMBIT. It was followed by the physical model, boundary conditions, and other appropriate parameters that were defined in the model's setup and solving stage. Finally the results could be obtained when FLUENT iterations led to converged results defined by a set of converged criteria. The temperature, heat transfer coefficient, and pressure drop across the pipe could be obtained throughout the computational domain in the post-process stage. FLUENT software is used to simulate governing equations of turbulent forced convection heat transfer in a horizontal tube with constant heat flux. The GAMBIT model is used to describe a problem which graphed and meshed the section test with a size of $0.02 \times 0.02 \times 1.6\ m^3$.

3. Computational method

3.1. Physical model

Cartesian geometry coordinates of the problem undertaken are shown in Fig. 1 and dimensions of the channel in Table 1. The boundary conditions of these study assumed steady state, incompressible and Newtonian turbulent fluid flow, constant thermophysical properties of nanofluids, no effect of gravity, heat conduction in the axial direction and neglecting the wall thickness.

A high Reynolds number has been estimated as the input parameter; the SIMPLE scheme of pressure treatment has been adopted, a turbulent viscous k–ε model has been employed, and converged solutions have been considered for residuals lower than 10^{-6} for all the governing equations. The results of the simulation for the nanofluid compared with the Blasius equation (12) for the friction factor and the Dittus–Boelter equation (Eq. (13)) for the Nusselt number are as follows:

$$f = \frac{0.316}{Re^{0.25}} \tag{12}$$

$$Nu = \frac{h_f}{k_f} D_{eff} = 0.023\, Re^{0.8}\, Pr^{0.4} \tag{13}$$

3.2. Governing equations

Infinitesimal (less than 100 nm) solid particles are assumed to have a single phase approach. For all these assumptions, the dimensional conservation equations for steady state mean conditions are as follows: continuity, momentum and energy equations Bejan [19].

$$\frac{\partial \overline{u}}{\partial x} + \frac{\partial \overline{v}}{\partial y} + \frac{\partial \overline{w}}{\partial z} = 0 \tag{14}$$

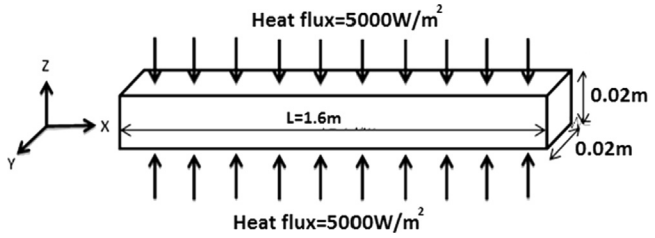

Fig. 1. Geometrical model.

Table 1
Geometrical parameters.

Parameters	Range (m)
Hydraulic diameter of duct (D_h)	0.02
Channel height (h)	0.02
Channel width (W)	0.02
Channel length (L)	1.6

$$\rho\left(\overline{u}\frac{\partial\overline{u}}{\partial x}+\overline{v}\frac{\partial\overline{u}}{\partial y}+\overline{w}\frac{\partial\overline{u}}{\partial z}\right)=-\frac{\partial\overline{p}}{\partial x}+\mu\nabla^2\overline{u}-\underline{\frac{\partial}{\partial x}\rho\overline{u^{12}}-\frac{\partial}{\partial y}\rho\overline{u'v'}-\frac{\partial}{\partial z}\rho\overline{u'w'}}$$

$$\rho\left(\overline{u}\frac{\partial\overline{v}}{\partial x}+\overline{v}\frac{\partial\overline{v}}{\partial y}+\overline{w}\frac{\partial\overline{v}}{\partial z}\right)=-\frac{\partial\overline{p}}{\partial y}+\mu\nabla^2\overline{v}-\underline{\frac{\partial}{\partial x}\rho\overline{u'v'}-\frac{\partial}{\partial y}\rho\overline{w^{12}}-\frac{\partial}{\partial z}\rho\overline{v'w'}}$$

$$\rho\left(\overline{u}\frac{\partial\overline{w}}{\partial x}+\overline{v}\frac{\partial\overline{w}}{\partial y}+\overline{w}\frac{\partial\overline{w}}{\partial z}\right)=-\frac{\partial\overline{p}}{\partial z}+\mu\nabla^2\overline{w}-\underline{\frac{\partial}{\partial x}\rho\overline{u'w'}-\frac{\partial}{\partial y}\rho\overline{v'w'}-\frac{\partial}{\partial z}\rho\overline{w^{12}}} \tag{15}$$

$$\rho c_p\left(\overline{u}\frac{\partial\dot{t}}{\partial x}+\overline{v}\frac{\partial\dot{t}}{\partial y}+\overline{w}\frac{\partial\dot{t}}{\partial z}\right)=k\nabla^2 t-\underline{\frac{\partial}{\partial x}\rho c_p\overline{u't'}-\frac{\partial}{\partial y}\rho c_p\overline{v't'}-\frac{\partial}{\partial z}\rho c_p\overline{w't'}} \tag{16}$$

3.3. Boundary conditions

The nanofluids' volume concentrations (1–4%) at 20 °C base temperature are used as an input. CFD analysis has been performed with a uniform velocity profile at the inlet and pressure outlet conditions used at the outlet of the channel. The turbulent intensity (I) is specified for an initial guess of turbulent quantities (k and ε). The turbulent intensity calculated for each case is based on the following formula:

$$I=0.16\,Re^{-1/8} \tag{17}$$

The walls of the tube are assumed to be perfectly smooth and the constant heat flux condition is specified on the inside tube wall with a value of 5000 W/m^2. The Reynolds number varied from 1×10^4 to 1×10^6 at each step of the iterations as the input data. The friction factor and the Nusselt number are introduced as the output data.

3.4. Grid independence test

The grid's independence in GAMBIT software for the channel as (40x40 × 160) cells and subdivisions in the axial length and surface face, respectively, is tested. To find the most suitable size of mesh faces, the grid independent test is performed for the physical model. In this study, rectangular cells are used to mesh the surfaces and wall of the channel. The grid independence is checked using different grid systems and four mesh faces are considered ($20\times20\times160$, $40\times40\times160$ and $20\times20\times200$) for pure water. The Nusselt number is estimated for all four mesh faces and the results were proper. Any number of mesh faces for these four cases can be used, but in this study, mesh faces with $40\times40\times160$ have been adopted as the best in terms of accuracy.

3.5. CFD simulation

The simulation results are tested by comparing with the predicted results of Refs. [11,21,22] that used circular heated tubes in the experimental work. The CFD modeling region could be classified into a few major steps: the preprocess stage, the geometry of the problem undertaken constructed as a square channel, and the computational mesh generated in GAMBIT. It was followed by the physical model, boundary conditions and other parameters appropriately defined in the model's setup and solving stage. All scalar values and velocity components of the problem are calculated at the center of the control volume interfaces where the grid schemes are used intensively. Throughout the iterative process accurate monitoring of the residuals was done. When the residuals for all governing equations were lower than 10^{-6}, all solutions were assumed to have converged. Finally, the results could be obtained when FLUENT iterations led to the converged results defined by a set of converged criteria. The friction factor and the Nusselt number inside the channel could be obtained throughout the computational domain in the post-process stage. The grid independent test of the Nusselt number against the Reynolds number with respect to all grid mesh sizes can be seen in Fig. 2. It seems that all the meshing sizes are proper but in this study, the mesh size $40\times40\times160$ will be considered as the optimum meshing size.

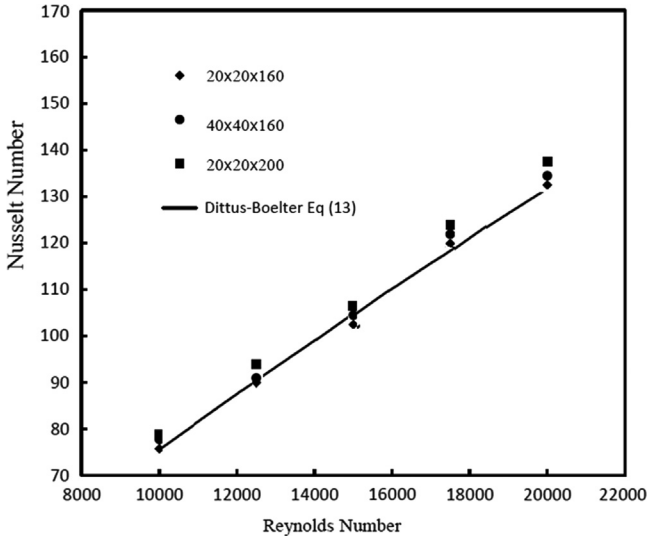

Fig. 2. Grid independent test.

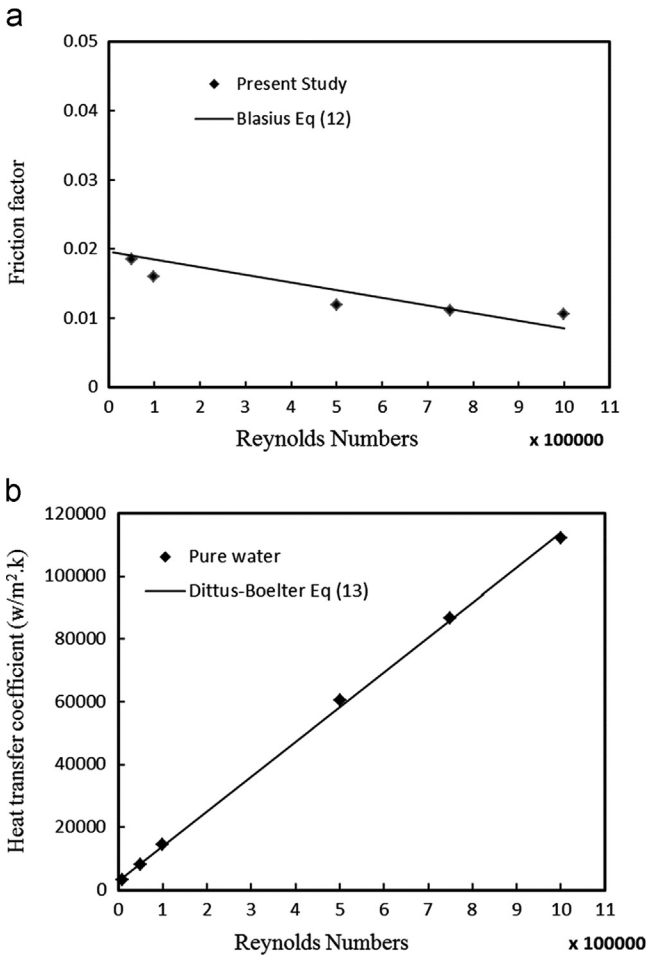

Fig. 3. Verification process.

4. Results and discussion

4.1. Verification process

The verification process is very important to check the results. It should be remembered that all CFD analysis runs were carried out at a constant temperature of 20 °C. It can be seen in Fig. 3a that the friction factor decreases with the increase of the Reynolds number under turbulent flow conditions. The Blasius equation (Eq. (12)) is indicated as a solid black line. It appears that there is good agreement among the CFD results and the equations. Likewise, the results of the heat transfer coefficient are shown in Fig. 3b. The heat transfer coefficient increases with the increase of the Reynolds number under turbulent flow conditions. The Dittus–Boelter equation (Eq. (13)) is also indicated as a solid black line. It appears that there is good agreement between the CFD analysis and the equation.

4.2. The effect of nanofluid type

Fig. 4a shows a comparison of the friction factor results for pure water and (CuO, TiO_2 and Al_2O_3) nanofluids at the turbulent regime. It seems insignificant affect of the types of nanofluids on the friction factor under turbulent flow conditions. Likewise, Fig. 4b indicates the Nusselt number with the Reynolds number for pure water and (CuO, TiO_2 and Al_2O_3) nanofluids at the turublent regime. It can be seen that CuO nanofluid has the highest values of the Nusselt number

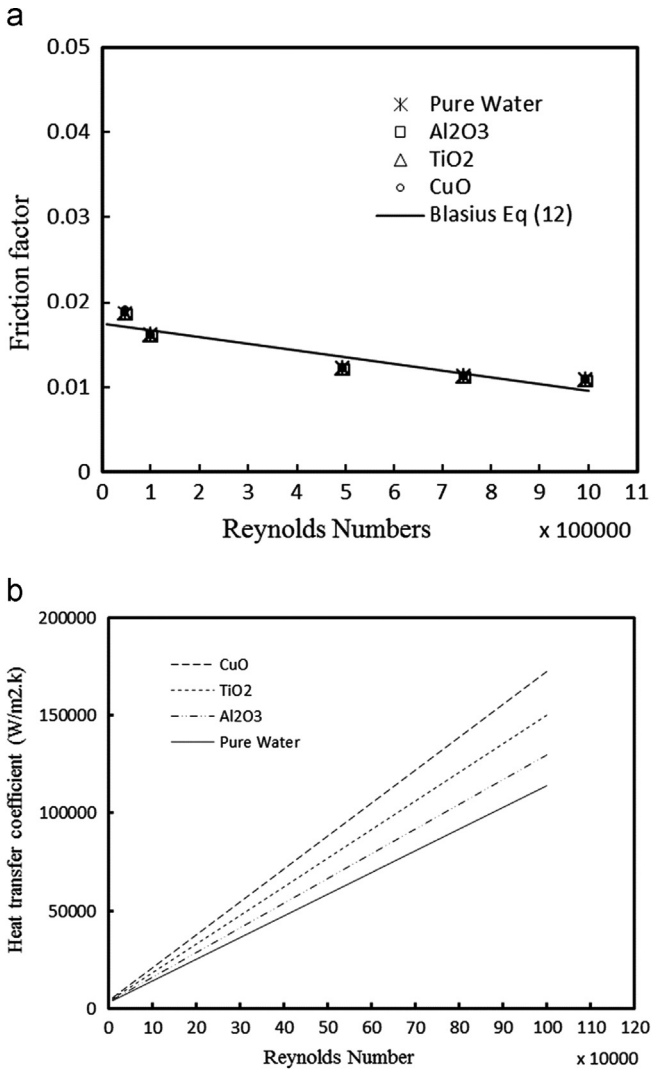

Fig. 4. Comparison of the computed values for pure water and nanofluids in the turbulent regime.

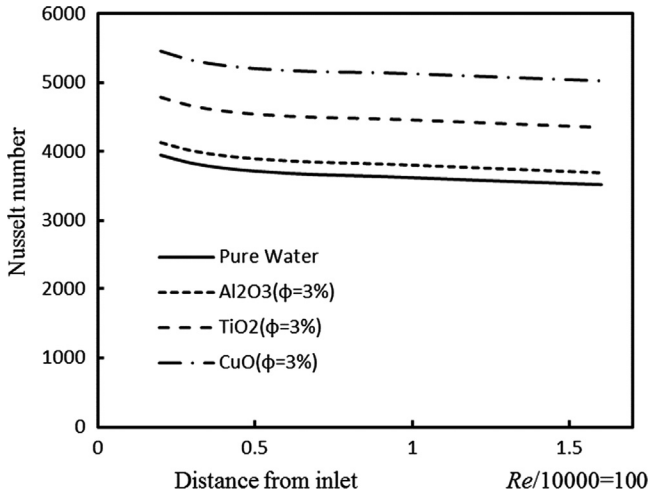

Fig. 5. Local Nusselt number with the length of the channel.

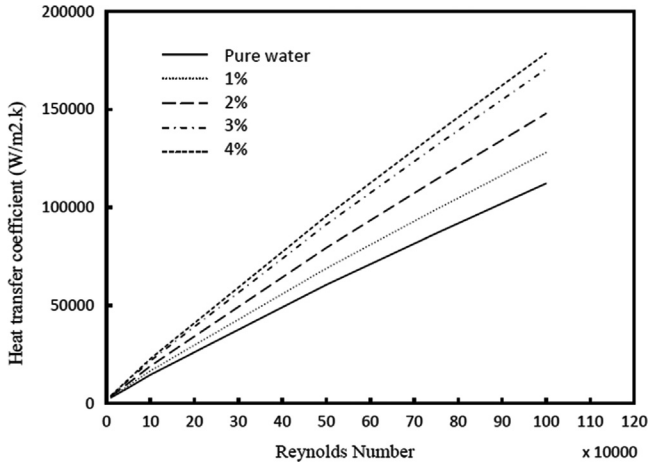

Fig. 6. The effect of nanofluid concentration on the heat transfer coefficient at the Reynolds number.

compared with others followed by TiO_2 and then Al_2O_3. The reason for the highest values of the Nusselt number for CuO may be the highest values of thermal conductivity and lowest viscosity. Also the Prandtl number of CuO has the highest value as compared with others.

Fig. 5 illustrates the local Nusselt number for CuO, TiO_2 and Al_2O_3 nanofluids with the volume fraction and nanoparticle diameter of 3% and 20 nm, respectively. The results indicate that increasing the Reynolds number can cause an increase in the local Nusselt number. This is due to the fact that a higher Reynolds number leads to a higher velocity and temperature gradient at the straight channel. It is clear that the behavior of CuO nanofluid is due to the optimum values of the Nusselt number. The reason may be related to the mixing caused by nanoparticles near the walls of the channel.

4.3. The effect of nanofluid volume fraction

The effect of the heat transfer coefficient with the Reynolds number for CuO nanofluid and 1–4% volume fraction is demonstrated in Fig. 6. It seems that the effect of the nanofluid volume fraction is significant. The heat transfer coefficient for pure water is also indicated as a solid black line. The maximum deviation is 60% when the volume fraction increased from 1% to 4%. The reason for increasing the heat transfer coefficient with an increase of the nanofluid volume fraction is the higher Prandtl number, thermal conductivity of nanoparticles and also a large energy exchange process resulting from the chaotic movement of the nanoparticles.

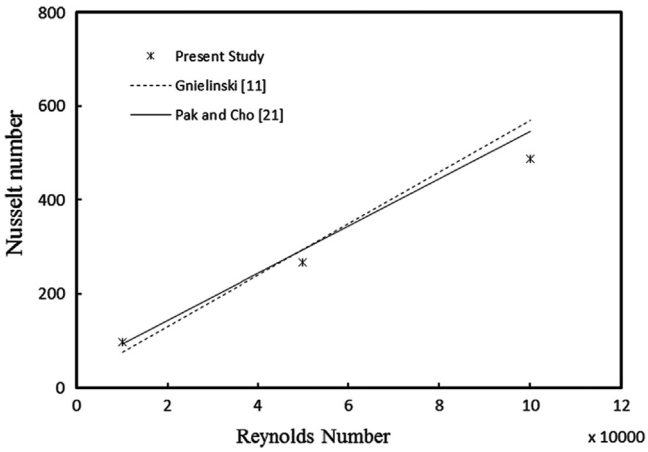

Fig. 7. Nusselt numbers' validation.

4.4. Validation

Fig. 7 shows a comparison of the simulation results of the Nusselt numbers and the equations given by Gnielinski [11] and Pak and Cho [21] for TiO_2 nanofluid. It can be seen that the Gnielinski and Pak and Cho correlations are indicated as a dashed black line and a solid black line, respectively. It seems that there is good agreement observed with the computed values from the theoretical equation, over the range of Reynolds numbers with a deviation of not more than 10%.

5. Conclusions

The thermal properties of three types of nanoparticles suspended in water were calculated depending on the equation of Ref. [13]. Forced convection heat transfer under turbulent flow is studied by numerical simulation with uniform heat flux boundary conditions of the straight channel. The heat transfer enhancement resulting from various parameters such as the nanoparticle concentration of volume and the Reynolds number is reported. Finite volume methods are used to solve the governing equations with certain assumptions and appropriate boundary conditions. The Nusselt number and friction factor are obtained through the numerical simulation. The study concluded that the enhancement of the friction factor and the Nusselt number is 2% and 21%, respectively, for the channel at all Reynolds numbers. The 4% volume concentration of nanofluid has the highest friction factor values, followed by 3%, 2% and 1%. The CFD analysis of pure water friction factor at the channel has higher values than the circular tube which was estimated from the Blasius equation. The Nusselt number of CuO has the highest value followed by TiO_2 and Al_2O_3. There is good agreement of the CFD analysis of the friction factor and the Nusselt number of the nanofluid with experimental data of Rostamani et al. [11] with a deviation of not more than 10%.

References

[1] Hussein AM, Sharma KV, Bakar RA, Kadirgama K. A review of forced convection heat transfer enhancement and hydrodynamic characteristics of a nanofluid. Renew Sustain Energy Rev 2014;29:734–43.
[2] Hussein AM, Bakar RA, Kadirgama K, Sharma KV. The effect of nanofluid volume concentration on heat transfer and friction factor inside a horizontal tube. J Nanomater; 2013:1–12 (article ID 859563, http://dx.doi.org/10.1155/2013/859563).
[3] Hussein AM, Bakar RA, Kadirgama K, Sharma KV. The effect of cross sectional area of tube on friction factor and heat transfer nanofluid turbulent flow. Int Commun Heat Mass Transf 2013;47:49–55.
[4] Meibodi ME. An estimation for velocity and temperature profiles of nanofluids in fully developed turbulent flow conditions. Int Commun Heat Mass Transf 2010;37:895–900.
[5] Hussein AM, Sharma KV, Bakar RA, Kadirgama K. Study of forced convection nanofluid heat transfer in the automotive cooling system. Case Stud Therm Eng 2014;2:50–61.
[6] Bahiraei M, Hosseinalipour SM, Zabihi K, Taheran E. Using neural network for determination of viscosity in water–TiO_2 nanofluid. Adv Mech Eng 2012: 1687–8132, http://dx.doi.org/10.1155/2012/742680.
[7] Bobbo S, Fedele L, Benetti A, Colla L, Fabrizio M, Pagura C, et al. Viscosity of water based SWCNH and TiO_2 nanofluids. Exp Therm Fluid Sci 2012;36: 65–71.
[8] Prajapati OS. Effect of Al_2O_3–water nanofluids in convective heat transfer. Int J Nanosci 2012;1:1–4.
[9] Bozorgan N, Mafi M. Performance evaluation of Al_2O_3/water nanofluid as coolant in a double-tube heat exchanger flowing under a turbulent flow regime. Adv Mech Eng 2012:1–8 (article ID 891382, http://dx.doi.org/10.1155/2012/891382).
[10] Luciu RS, Mateescu T, Cotorobai V, Mare T. Nusselt number and convection heat transfer coefficient for a coaxial heat exchanger using Al_2O_3–water ph=5 nanofluid. Bul Inst Politeh Ias¸i 2009;2 (t. LV (LIX), f.).
[11] Rostamani M, Hosseinizadeh SF, Gorji M, Khodadadi JM. Numerical study of turbulent forced convection flow of nanofluids in a long horizontal duct considering variable properties. Int Commun Heat Mass Transf 2010;37:1426–31.
[12] Hussein AM, Bakar RA, Kadirgama K, Sharma KV. Experimental measurements of nanofluids thermal properties. Int J Automot Mech Eng 2013;7: 850–64.

[13] Sundar LS, Sharma KV. Turbulent heat transfer and friction factor of Al_2O_3 nanofluid in circular tube with twisted tape inserts. Int J Heat Mass Transf 2010;53:1409–16.
[14] Dehghandokht M, Khan MG, Fartaj A, Sanaye S. Flow and heat transfer characteristics of water and ethylene glycol–water in a multi-port serpentine meso-channel heat exchanger. Int J Therm Sci 2011;50:1615–27.
[15] Oliet C, Oliva A, Castro J, Segarra SD. Parametric studies on automotive radiators. Appl Therm Eng 2007;27:2033–43.
[16] Leong KY, Saidur R, Kazi SN, Mamun AM. Performance investigation of an automotive car radiator operated with nanofluid-based coolants (nanofluid as a coolant in a radiator). Appl Therm Eng 2010;30:2685–92.
[17] Gunnasegaran P, Shuaib NH, Abdul Jalal MF, Sandhita E. Numerical study of fluid dynamic and heat transfer in a compact heat exchanger using nanofluids. Int Sch Res Netw Mech Eng 2012;2012:1–11.
[18] Durmus A, Esen M. Investigation of heat transfer and pressure drop in a concentric heat exchanger with snail entrance. Appl Therm Eng 2002;22: 321–32.
[19] Bejan A. Convection heat transfer. New York: John Wiley & Sons Inc.; 2004.
[21] Pak BC, Cho YI. Hydrodynamic and heat transfer study of dispersed fluids with submicron metallic oxide particles. Exp. Heat Transf 1998;11:70–151.
[22] Duangthongsuk W, Wongwises S. An experimental study on the heat transfer performance and pressure drop of TiO_2–water nanofluids flowing under a turbulent flow regime. Int J Heat Mass Transf 2010;53:334–44.